

1 **CO₂ and CH₄ exchanges between moist moss tundra and atmosphere on Kapp**
2 **Linne, Svalbard**

3 **Anders Lindroth¹, Norbert Pirk², Ingibjörg S Jónsdóttir³, Christian Stiegler⁴, Leif**
4 **Klemedtsson⁵, and Mats B Nilsson⁶**

5 ¹Department of Physical Geography and Ecosystem Science, Lund University, Lund, Sweden.

6 ²Department of Geosciences, University of Oslo, Oslo, Norway.

7 ³Life and Environmental Sciences, University of Iceland, Reykjavik, Iceland.

8 ⁴Bioclimatology, Georg-August Universität Göttingen, Göttingen, Germany.

9 ⁵Department of Earth Sciences, University of Gothenburg, Gothenburg, Sweden.

10 ⁶Department of Forest Ecology and Management, Swedish University of Agricultural Sciences,
11 Umeå, Sweden.

12 Corresponding author: anders.lindroth@nateko.lu.se

13 Abstract

14 We measured CO₂ and CH₄ fluxes using chambers and eddy covariance (only CO₂) from a moist
15 moss tundra in Svalbard. The average net ecosystem exchange (NEE) during the summer (9
16 June-31 August) was negative (sink) with $-0.139 \pm 0.032 \mu\text{mol m}^{-2}\text{s}^{-1}$ corresponding to -11.8 g C
17 m^{-2} for the whole summer. The cumulated NEE over the whole growing season (day no. 160 to
18 284) was -2.5 g C m^{-2} . The CH₄ flux during the summer period showed a large spatial and
19 temporal variability. The mean value of all 214 samples was $0.000511 \pm 0.000315 \mu\text{mol m}^{-2}\text{s}^{-1}$
20 which corresponds to a growing season estimate of 0.04 to $0.16 \text{ g CH}_4 \text{ m}^{-2}$. Thus, we find that
21 this moss tundra ecosystem is closely in balance with the atmosphere during growing season
22 when regarding exchanges of CO₂ and CH₄. The sink of CO₂ as well as the source of CH₄ are
23 small in comparison with other tundra ecosystems in high Arctic.

24
25 Air temperature, soil moisture and greenness index contributed significantly to explain the
26 variation in ecosystem respiration (R_{eco}) while active layer depth, soil moisture and greenness
27 index were the variables that best explained CH₄ emissions. Estimate of temperature sensitivity
28 of R_{eco} and gross primary productivity (GPP) showed that the sensitivity is slightly higher for
29 GPP than for R_{eco} in the interval $0 - 4.5 \text{ }^\circ\text{C}$, thereafter the difference is small up to about $6 \text{ }^\circ\text{C}$ and
30 then it began to raise rapidly for R_{eco} . The consequence of this, for a small increase in air
31 temperature of 1 degree (all other variables assumed unchanged) was that the respiration
32 increased more than photosynthesis turning the small sink into a small source (4.5 g C m^{-2}) during
33 the growing season. Thus, we cannot rule out that the reason why the moss tundra is close to
34 balance today is an effect of the warming that has already taken place in Svalbard.

35 1 Introduction

36 Climate warming is predicted to be most evident at high latitudes (Friedlingstein et al., 2006)
37 with profound effects on ecosystem functioning. One of the high latitude regions that are
38 expected to experience the most dramatic changes caused by climate change is the Arctic. This
39 region which is located roughly north of the tree-line is characterized by cold winters and cool
40 summers and with mean annual temperatures below zero. The summer periods are short ranging
41 between 3.5 to 1.5 months from the southern boundary to the north and July is normally the
42 warmest month. Annual precipitation is generally low decreasing from about 250 mm in the
43 southern areas to 45 mm in polar deserts in the north (Callaghan et al., 2005).

44
45 The permafrost soils in the Arctic store $1035 \pm 150 \text{ Pg}$ of organic carbon in the top 0-3 m
46 (Hugelius et al., 2014) which is more than the average 2010-2019 of 860 Pg of carbon in the
47 atmosphere (Friedlingstein et al., 2020). The increased warming in these areas can induce higher
48 decomposition rates due to increased microbial activity which will provide a positive feedback to
49 the climate system (Schuur et al., 2015). On the other hand, warming can also increase
50 photosynthesis and carbon uptake and thus compensate for, or exceed, the effect of increased
51 decomposition. Climate warming is also affecting plant community composition and the length
52 of the growing season (Post et al., 2009) which also has an impact on the processes regulating
53 annual carbon emissions and uptake (Bosiö et al., 2014). There is however a large uncertainty
54 regarding the timing, magnitude and possible sign of potential feedbacks caused by these
55 changes (Myers-Smith et al., 2020).

56

57 Understanding processes that are controlling the exchanges of greenhouse gases in the Arctic is
58 crucial for assessment of potential feedback effects. For this purpose, multiple year-around long-
59 term studies including direct measurements of CO₂ and CH₄ fluxes covering all seasons, winter,
60 spring, summer and autumn would be ideal. This is a great challenge in the harsh climate of the
61 Arctic and with limited support of key infrastructures for, e.g., provision of electricity for
62 operation of instruments.

63
64 In spite of these difficulties a few year-around studies have been performed during the last
65 couple of decades. In the low Arctic, Oechel et al. (2013) demonstrate the importance of the
66 wintertime fluxes in a tussock tundra ecosystem in Alaska. They found that the non-summer
67 season emitted more CO₂ than the corresponding uptake during the summer resulting in a net
68 source to the atmosphere of about 14 g C m⁻² on an annual basis. They also showed that the
69 shoulder seasons, spring and autumn roughly out-weighted the summer uptake. Euskirchen et al.
70 (2012, 2016) measured net CO₂ exchange in three different tundra ecosystems; heath tundra,
71 tussock tundra and wet sedge tundra in northern Alaska over three years. They found that the
72 uptake of -51 to -95 g C m⁻² during the summer (June-August) was overturned by the respiration
73 that occurred during the winter period resulting in net annual losses for all three ecosystems.
74 Zhang et al. (2019) reported five years of year-around flux measurements in a heath ecosystem
75 on west Greenland and they found that the heath was an annual sink of -35±15 g C m⁻². One year
76 with an anomalously deep snow pack showed a 3-fold higher respiration during the winter as
77 compared to the other years which resulted in a significantly lower net uptake during that year.

78
79 Even fewer studies have been done on year-around studies in the high Arctic. Lüers et al. (2014)
80 quantified the annual CO₂ budget using eddy covariance measurements in a river catchment area
81 near Ny-Ålesund on Spitsbergen in the Svalbard archipelago and they found that the ecosystem
82 was in C-balance. The footprint area was a semi-polar desert with only 60% vegetation cover and
83 patches of bare soil and stones. Also in Svalbard but further south in Adventdalen on a flat
84 alluvial fen irregularly covered with ice wedged polygons, Pirk et al. (2017) made year-around
85 measurements of CO₂ fluxes and found it to be a net sink of -82 g C m⁻². Because of the
86 irregularities caused by the ice wedges and the differences in wetness, they focused the analyses
87 on the spatial variability in two different directions, one wetter and one drier, and they estimated
88 the annual net ecosystem exchange to -91 g C m⁻² and -62 g C m⁻² for the respective areas.

89
90 The Arctic ecosystems constitute also a source of CH₄ to the atmosphere even if it is not a very
91 large one. Saunois et al. (2020) estimated that the Northern high latitude region (60°N - 90°N)
92 contributed 4% of global emissions and emissions from wetlands are only part of the emissions
93 from this region. However, in the light of the vulnerability of the high Arctic permafrost areas
94 and considering the large carbon pool and the predicted changes in climate, a quantification and
95 understanding of CH₄ exchanges in these areas are still important. Christensen et al. (2004)
96 showed one example of a dramatic impact of the climate warming on the CH₄ emissions in a
97 permafrost mire in sub-arctic Sweden. The warming which is visible in this area since decades
98 and its impact on permafrost and vegetation changes was estimated to have caused an increase of
99 landscape CH₄ emissions in the range 22-66% in the period 1970 to 2000.

100
101 Mastepanov et al. (2008) were the first to show the importance of emissions also outside of the
102 growing season. They observed a large burst of CH₄ from a fen area in Zackenberg, Greenland

103 after the growing season and during the time when the soil started to freeze. This finding was
104 confirmed in a later paper (Mastepanov et al., 2013) and the process was hypothetically
105 attributed to the subsurface CH₄ pool. Hydrology and vegetation composition play an important
106 role for CH₄ emission and dynamics. McGuire et al. (2012) made a comprehensive summary of
107 CH₄ exchanges of the Arctic tundra showing the difference between wet and dry ecosystems; the
108 wet tundra emitted 5.4 to 13.0 g CH₄-C m⁻² during summer and 8.5 to 20.2 g CH₄-C m⁻²
109 annually. The corresponding values for the dry/mesic tundra were 0.3 to 1.4 g CH₄-C m⁻² and 0.3
110 to 4.3 g CH₄-C m⁻², respectively. Bao et al. (2021) utilized year-around measurements of CH₄
111 fluxes from three sites of the Ameriflux network in Northern Alaska to demonstrate the
112 importance of the spring and autumn seasons for the annual emission. The shoulder seasons
113 contributed about 25% of the annual emissions and the autumn season had about three times
114 higher emission than the spring season. These findings increasingly emphasise the importance of
115 year-around measurements to fully understand the CH₄ controls and dynamics.

116

117 The main aim of this study is to provide another piece of the puzzle concerning CO₂ and CH₄
118 exchanges from different but widespread ecosystem types in the high Arctic. We hypothesise
119 that this moist tundra ecosystem is a net carbon sink during the growing season and that the
120 summer emissions of methane will be at levels comparable with other methane emitting high
121 Arctic ecosystems. We made flux measurements of CO₂ and CH₄ in an moist moss tundra
122 ecosystem situated at Kapp Linne on the west coast of the Svalbard archipelago in 2015 and with
123 an additional campaign in 2016. The measurements in 2015 were done using both eddy
124 covariance system (CO₂) and chambers (CO₂ and CH₄) but only chambers in 2016. We quantify
125 ecosystem respiration (R_{eco}), gross primary productivity (GPP) and net ecosystem exchange
126 (NEE) during the growing season based on a combination of chamber end eddy covariance
127 measurements. The CH₄ emission was only quantified for the summer season. We also analyze
128 the environmental controls of the fluxes.

129 **2 Materials and Methods**

130 **2.1 Research site and measurements**

131

132 This study was performed in the Svalbard archipelago near the weather station Isfjord Radio
133 (78°03'08" N 13°36'04" E, alt. 7 m) which is located right on the foreland of Kapp Linné on the
134 island of Spitzbergen (Fig. S1). The tundra area where the measurements were performed is
135 located about 1 km southeast of the station. The study area consists of moist moss tundra, a
136 widespread ecosystem in Svalbard (Vanderpuye et al., 2002; Ravolainen et al., 2020). The
137 vegetation is characterised by the moss species *Tomentypnum nitens*, *Sanionia uncinata* and
138 *Aulacomium palustre* and a sparse cover of vascular plants (20-40%), dominated by *Equisetum*
139 *arvense*, *Salix polaris* and *Bistorta vivipara*. Other vascular plant species found in the plots:
140 *Saxifraga cespitosa*, *Saxifraga oppositifolia*, *Silene aucaulis*, and some grass species, most likely
141 *Alopecurus ovatus* (previously *A. borealis*), and *Poa arctica*. The vegetation analysis was made
142 from photographs of chamber location plots taken between 26 June and 2 July 2015 (see Figs.
143 S4a-4y in Supplement).

144

145 The net ecosystem exchange of CO₂ was measured with an eddy covariance (EC) system located
146 centrally on the moss tundra (78°03'28.6" N 13°38'40" E). The sonic anemometer (USA-1;

147 Metek GmbH, Germany) was mounted on top of a tripod (see Fig. S1) at 2.7 m height. The CO₂
148 and H₂O concentrations were measured with an open path sensor (LI-7500; Li-Cor Inc., USA)
149 placed just beneath the sonic and inclined about 30° pointing towards east. Radiation
150 components, incoming and outgoing short-wave and long-wave (CNR-4; Kipp & Zonen, the
151 Netherlands) were measured at 2.0 m height above ground with the sensor directed towards
152 south. All sensors were connected to a datalogger (CR-1000; Campbell Scientific, USA) which
153 was powered by a solar panel and a battery. The EC sensors were sampled and stored at 10 Hz
154 and all other sensors were sampled at 0.1 Hz with storage of 30 min mean values. These
155 measurements were made from 25 June to 17 September 2015. The total data coverage during
156 this period was 47% with a longer break in the measurements between 28 July and 29 August.

157
158 The soil efflux of CO₂ and CH₄ was measured with a dark chamber connected to a gas analyzer
159 (Ultraportable Greenhouse Gas Analyzer; Los Gatos Research, USA) on 24 locations within the
160 EC average footprint area. A circular thin-steel frame, 15 cm in diameter and 15 cm high, was
161 inserted ca 5 cm into the ground in each location. The sharp edge of the frames made it easy to
162 insert them into the ground without damaging the vegetation and with minimal soil disturbance.
163 A picture was taken of each frame (see Supplement) for documentation of vegetation and for
164 calculation of different indexes. The chamber was also made from steel and it had a rubber seal
165 in the end facing the frame (Fig. S2) to make it air tight when mounted on the frame. The volume
166 of the chamber and the part of the frame raised above the surface was 5.3 L. A small fan was
167 installed inside the chamber to provide good mixing of the air during measurement. A small
168 weight (stone) was placed on top of the chamber during measurement to prevent it from moving
169 due to wind gusts. During concentration measurement air was circulated in a closed loop
170 between the chamber and the gas analyzer in ca. 10 m long 4 mm diameter polyethene tubes (see
171 Fig. S2). The air flow through the analyzer was ca 1.2 L min⁻¹. The chamber was ventilated in
172 the free air about 1 minute before each measurement which lasted for 5 minutes. The
173 concentrations were recorded and stored once per second by the gas analyzer. The time stamp of
174 the recorded data was used to identify measurement cycles for analysis of fluxes.

175
176 The chamber measurement positions were selected in the following way. The frames were
177 grouped in two sections, one north-east and one south-west of the flux tower since it was
178 expected that the main wind direction would be along that direction. Each group was then split
179 into three subsections with four measurement points within each one of them. The locations were
180 named S1:1-S1:4, S2:1-S2:4, S3:1-S3:4, N1:1-N1:4, N2:1-N2:4 and N3:1-SN3:4. The four
181 measurement points within each subsection were then placed along a transect with 3-4 m
182 between each point. This way it was possible to measure all four chamber locations without
183 having to move the whole measurement system. Chamber measurements were made in three
184 separate campaigns: mid-summer (26 June to 2 July 2015), late-summer (25-27 August 2015)
185 and early-summer (14-15 June 2016). Each location was measured three times during each one
186 of the three campaigns, a total of 216 measurements. Besides gas concentrations, also soil
187 temperature (5 cm), soil moisture (0-5 cm) and active layer depth was measured during each
188 campaign.

189
190 Meteorological data needed for analyses and gap-filling were obtained as follows: Hourly air
191 temperature and relative humidity from Isfjord radio, half-hourly global radiation from
192 Adventdalen, daily snow depth and ground ice conditions from Svalbard airport and monthly

193 precipitation from Isfjord radio and Barentsburg. The distance between the measurement site and
194 these stations are; Isfjord radio, 1 km, Barentsburg, 13 km, Svalbard airport, 46 km and
195 Adventdalen, 50 km. Using data from the more distant locations, Svalbard airport and
196 Adventdalen, introduces some additional uncertainty. Concerning global radiation data we could
197 compare in situ measured half-hourly radiation with the corresponding data from Adventdalen
198 for a shorter period and it showed general good agreement although with relatively large scatter
199 ($y = 0.84x + 15.9$; $r^2=0.57$; $n=580$). According to Dobler et al. (2021) the amount of precipitation
200 in the area where Kapp Linne and Svalbard airport are located don't show any significant
201 differences on an annual basis. Vickers et al. (2020) analysed timing of snow cover in Svalbard
202 and they show that the mean (2000-2019) first snow-free day is very similar in areas where Kapp
203 Linne and Svalbard airport are located. Thus, we are confident that using data from these
204 relatively remote locations does not introduce serious bias in our analyses. Data sources are
205 given in Acknowledgement.

206

207 **3. Data analysis**

208

209 The rawdata from the eddy covariance flux measurements were analysed using the Eddypro
210 software version 6.1.0 (Li-Cor, 2016). Correction was made for the impact of the additional heat
211 flux in the sensor path of the open path analyzer on the flux calculations according Burba et al.
212 (2008). Gap filling during the measurement period was made using the REddyProc online eddy
213 covariance data processing tool developed at the Max Planck Institute for Biogeochemistry
214 (Wutzler et al., 2018) without u^* correction since we could not identify any threshold for u^* . The
215 u^* threshold is generally low for low and smooth vegetation (Pastorello et al., 2020) and for a
216 wind exposed site as ours, it is not surprising that such threshold could not be found. Flux
217 partitioning was made with the daytime-based method according Lasslop et al. (2000). Only data
218 of highest quality, i.e. class=0 was retained for the gap filling and further analyses. Gap filling
219 outside of the EC measurement period to obtain the carbon balance for a full growing season was
220 made using empirical relationships for R_{eco} and GPP (see below).

221

222 For flux footprint calculations the roughness length (z_0) is needed and it was calculated from the
223 wind profile relationship in near neutral ($-0.01 < z/L < 0.01$) conditions:

224

$$225 \quad z_0 = \frac{z_m}{e^{(u(z) \frac{k}{u^*})}} \quad (1)$$

226

227 where z_m is measurement height, $u(z)$ is wind speed at height z , k is von Karman's constant and
228 u^* is friction velocity. We used the flux footprint prediction (FFP) online tool by Kjun et al.
229 (2015) to calculate the footprint climatology.

230

231 The fluxes from the chamber measurements were estimated from the time change of the
232 concentrations using linear regression. Every individual measurement was inspected and
233 evaluated manually. These inspections showed that 50 seconds for CO_2 and 100 seconds for CH_4
234 were optimal to obtain near perfectly linear responses a few seconds after the chamber had been
235 placed on the frame. The slopes of the regressions were then used to calculate fluxes per unit
236 surface area. The flux detection limits for CO_2 and CH_4 were calculated in the following way:
237 first the peak-to-peak variation in the respective gases were determined when the chamber was
238 ventilated in the free air and when conditions were steady. Then 20 sets of artificial 'fluxes' for

239 each gas species were estimated based on 100 randomly generated concentrations for each data
240 set. The peak-to-peak difference was used as seed (input) for the randomly generated values. The
241 95% value of the distribution of these randomly generated fluxes was taken as the flux detection
242 limit for the respective gas.

243
244 The pictures of the vegetation inside of the chamber frames were analysed using the ImageJ
245 (<https://imagej.net>) public domain software. The camera color channel information (digital
246 numbers for Red (R), Green (G) and Blue (B) channels) was collected from the JPEG pictures.
247 This type of pictures is for instance used in studies that are tracking the phenological
248 development of vegetation (e.g. Richardson et al., 2009). The so-called green index (GI) is
249 applied to detect differences in greenness of vegetation:

$$250$$
$$251 \quad GI = G/(R+G+B) \quad (2)$$
$$252$$

253 This index was also estimated for the central footprint area (100 m radius) of the flux
254 measurement location using a picture taken at 160 m above the altitude of the measurement area.

255 Forward stepwise linear regression (Sigmaplot 12.5) was used to analyze the dependency of the
256 CO₂ and CH₄ fluxes on environmental variables. We tested for air temperature (T_a), soil moisture
257 (θ), soil temperature (T_s), active layer depth (ALD), measurement location (S_{id}) and GI.

258
259 For gap filling of R_{eco} we only had access to air temperature with full annual coverage and, thus,
260 we could only use this driver for estimation of the R_{eco}. The measured chamber CO₂ fluxes were
261 fitted to the Lloyd & Taylor (1994) model with air temperature (T_a) as independent variable:

$$262$$
$$263 \quad FCO_2 = a \cdot e^{b \left(\frac{1}{56.02} - \frac{1}{T_a + 46.02} \right)} \quad (3)$$
$$264$$

265 During the EC measurement period (25 June to 17 September 2015) the GPP was estimated as:

$$266$$
$$267 \quad GPP = NEE_f - R_{eco} \quad (4)$$
$$268$$

269 Where NEE_f is the gap filled NEE according to Wutzler et al. (2018). This way R_{eco} and GPP
270 become consistent with the measured and gap filled NEE. For the time before and after this
271 period NEE was estimated as the sum of modelled R_{eco} and modelled GPP. The data for the GPP
272 model was derived from:

$$273$$
$$274 \quad GPP_m = NEE_m - R_{eco} \quad (5)$$
$$275$$

276 Where NEE_m is the measured net ecosystem exchange. The GPP_m was then fitted to a light
277 response function:

$$278$$
$$279 \quad GPP_m = c1 + c2 \cdot c3 / (c2 + R_g) \quad (6)$$

280

281 4 Results

282 For CO₂ exchanges and partitioning we combined the soil efflux measurements with the chamber
283 system with the eddy covariance flux measurements. This was crucial for the partitioning and for
284 gap filling because from 20 April to 20 August at this location the sun is above the horizon 24
285 hours of the day and this means that there were few occasions of dark nighttime measurements
286 with the eddy covariance system and all of these were collected at the very end of the summer.
287 We consider the chamber measurements that were distributed across the summer to be more
288 representative of R_{eco} for this location.

289

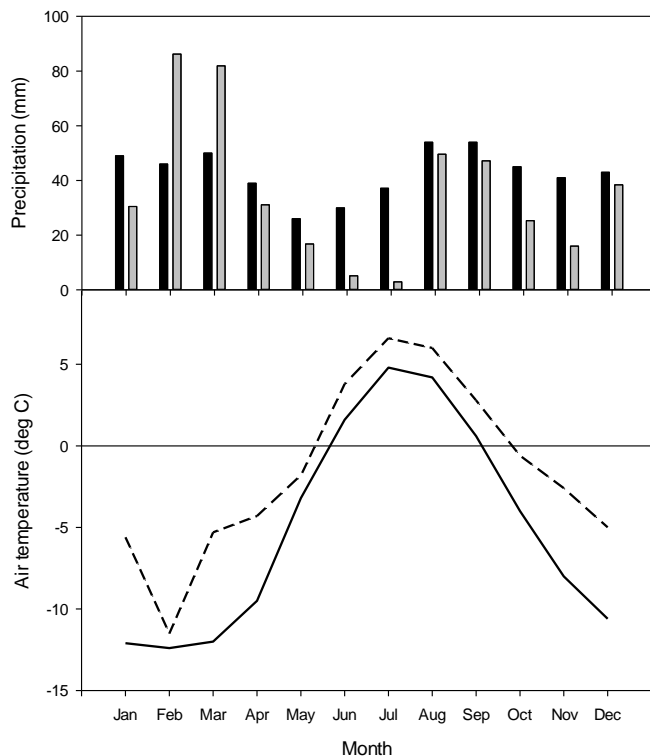
290 For CH₄ exchanges we don't have any eddy covariance measurements so we present only
291 chamber data for this variable.

292

293 4.1 Weather

294

295 The mean annual temperature at Kapp Linne was -1.5 °C during 2015 which was 3.5 °C higher
296 than the long-term mean (1961-1990) of -5.1 °C. The summer (June-August) mean of 5.5 °C was
297 2.0 °C higher than the long-term mean for the same time period (Fig. 1). The summer
298 precipitation in 2015 was much lower, 58 mm as compared to the long-term precipitation which
299 was 121 mm. The annual precipitation was also lower, 431 mm compared to the long-term
300 precipitation which was 514 mm.



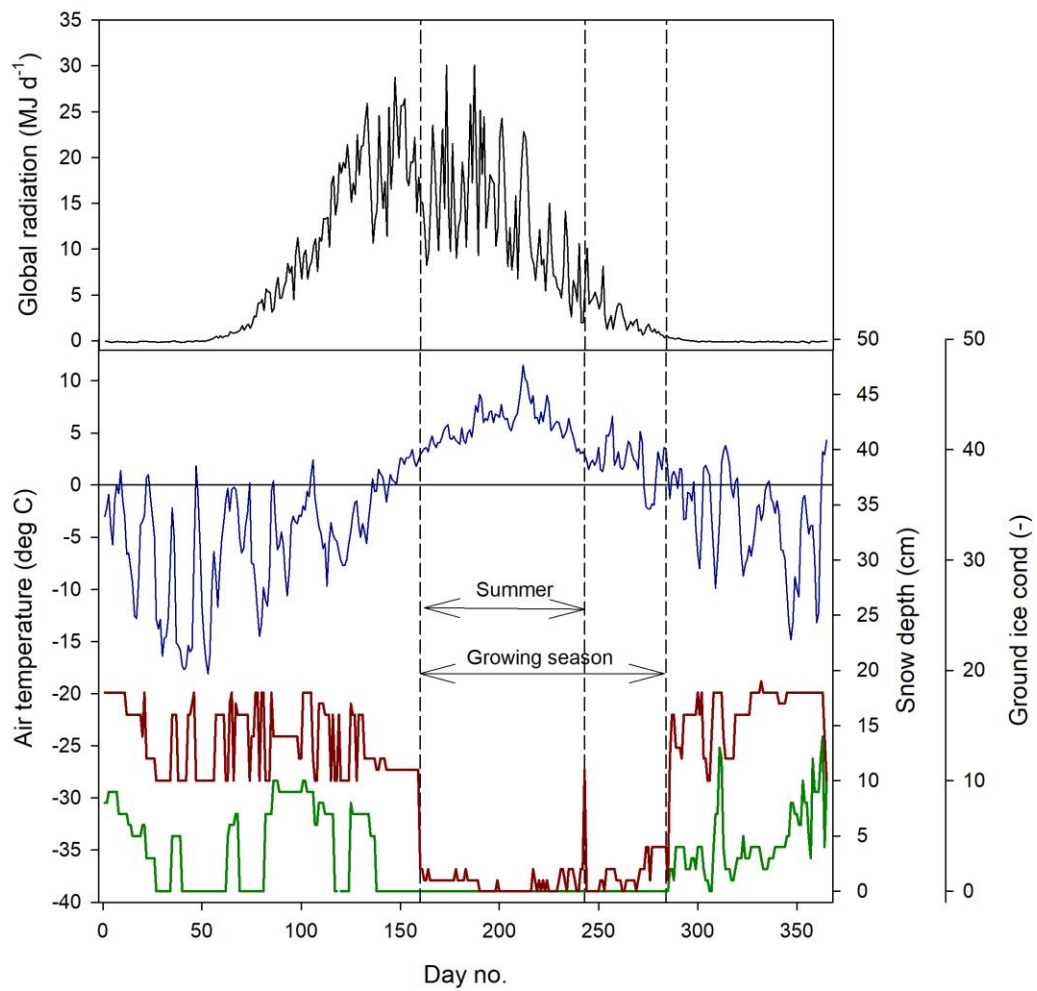
301
302 Figure 1. Monthly precipitation (top): Long-term average 1961-1990 black bars and 2015 grey
303 bars. Data from Barentsburg for January-May, from Isfjord Radio for June-December. Mean

304 monthly air temperature (bottom): Solid line is long-term average 1961-1990 and dotted line is
305 2015. Data from Isfjord Radio which is located about 1 km west of the investigation area.

306

307 We defined the growing season (the period during which vegetation is photosynthesizing) based
308 on the permanence of the snow pack which resulted in start day no. 160 and end day no. 284
309 (Fig. 2). The summer period which normally is defined as June through August was here defined
310 as lasting between 9 June (same as start of growing season) until end of August (Fig.2).

311



312
313

314 Fig. 2 Weather conditions during 2015. Top panel: Mean daily global radiation at Adventdalen.
315 Bottom panel: Mean daily air temperature at Isfjord Radio (blue), snow depth (red) and ground

316 ice conditions (green) at Svalbard airport close to Longyearbyen. The ground ice condition is
317 scaled from 0 to 20 where 0 is no snow or ice on the ground and 20 indicate a complete cover of
318 snow or ice.

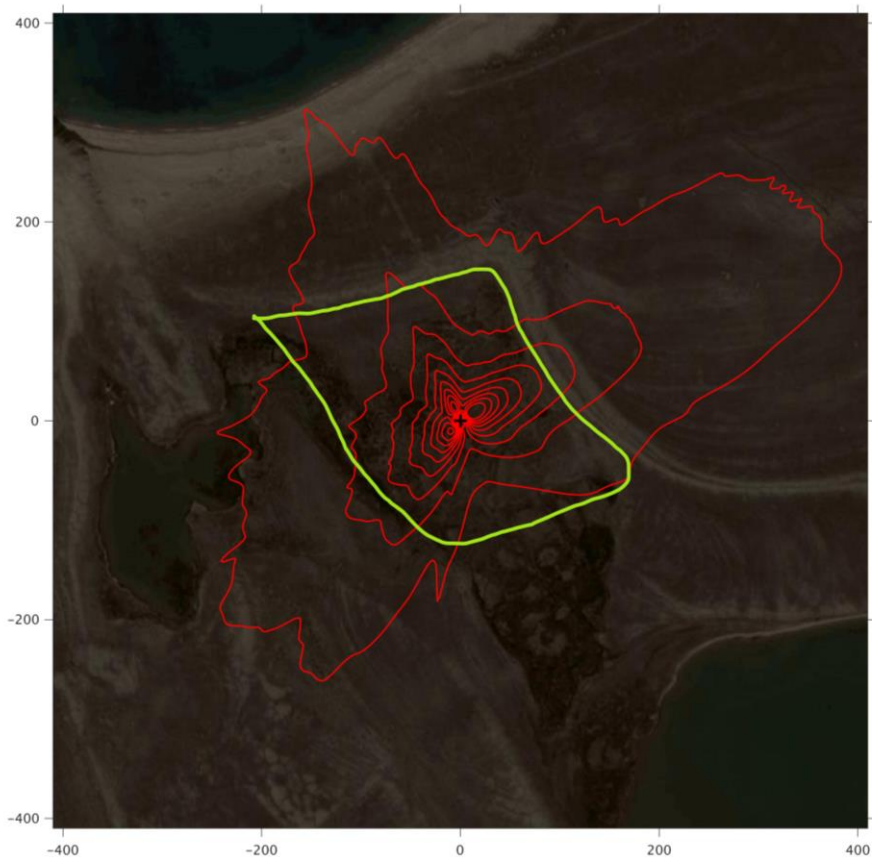
319

320 4.2 Flux footprint and greenness

321

322 The footprint climatology shows a good representativity of the moss tundra surface by the EC
323 measurements with 60-70% of fluxes emanating from areas well within the border of the tundra
324 (Fig. 3). The mean green index for a circular area with radius of 100 m centered at the flux tower
325 was 0.34 which corresponded exactly to the mean value for all chamber locations. The GI for the
326 24 chamber locations varied between 0.316 and 0.369. We observed a good (visual) correlation
327 between GI and coverage of green plants (see Figures S4a-S4y of chamber location pictures and
328 GI).

329



330

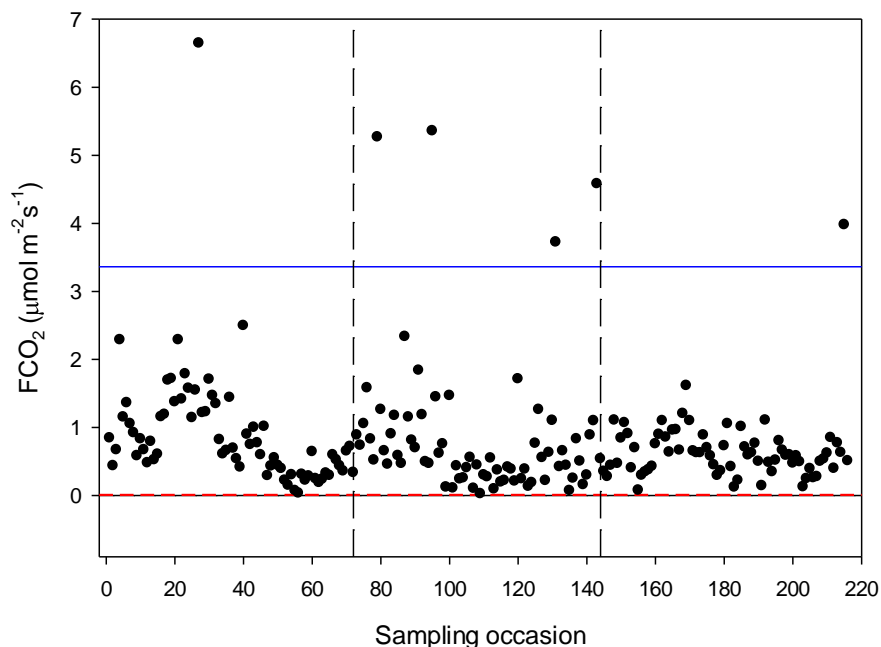
331 Figure 3. The footprint climatology with red contour lines 10-90%. The area within the green
332 line mark the heart of the moss tundra. The scale (m) is shown on the outer borders of the
333 picture.

334

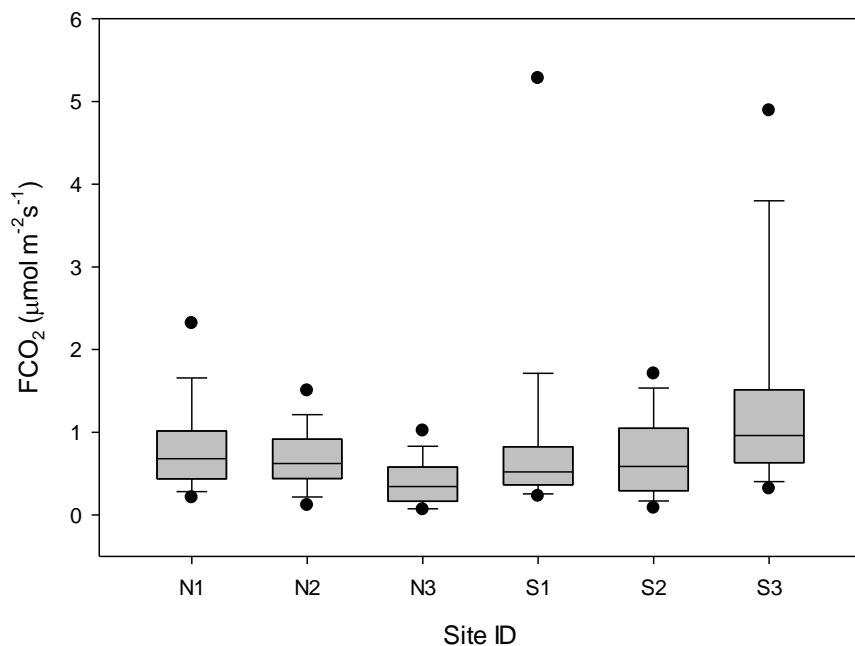
335 4.3 CO₂ exchanges

336

337 The CO₂ fluxes from the chamber measurements showed quite large variation over time (Fig. 4)
338 and across sampling locations (Fig. 5). The mean CO₂ flux of all samples was $0.81 \pm 0.11 \mu\text{mol m}^{-2}\text{s}^{-1}$.
339 The uncertainty is given as the 95 confidence limit.
340



341
342 Figure 4. Measured CO₂ exchange (FCO₂) from the 24 sampling points using dark chamber and
343 portable gas analyzer. The dashed red line indicates CO₂ flux detection limit and the blue line
344 represents 3xS.D. of all data points. The dashed vertical lines separate sampling periods from left
345 to right: 14-15 June, 26 June – 2 July and 25-27 August, respectively.



346

347 Figure 5. Box plot of CO₂ fluxes (FCO₂) per sampling location named N1-N3, S1-S3. The
 348 boundaries of the grey boxes represent the 25% and 75% percentiles, the line represent the
 349 median, whiskers above and below the boxes indicate the 10% and 90% percentiles. Outlying
 350 points are also shown.

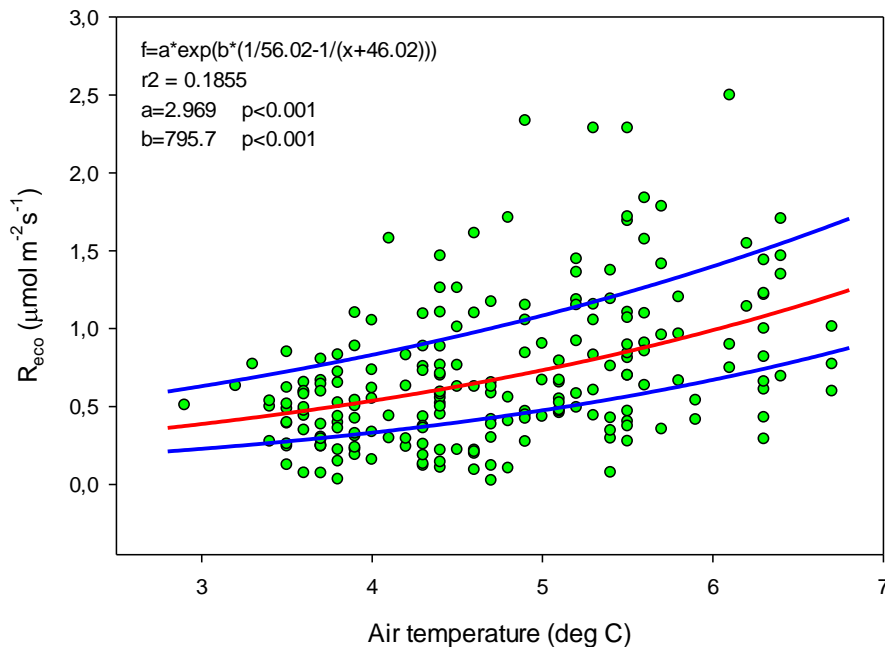
351
 352 Of the tested environmental variables T_a, θ, T_s, ALD, S_{id} and GI it was only T_a, θ and GI that
 353 contributed positively and significantly in decreasing order to explain the variability of the CO₂
 354 flux (Table 1).

355
 356 Table 1. Result of stepwise linear regression with CO₂ flux as dependent variable. Normality test
 357 failed but significance in all variables was confirmed with Wilcoxon Signed rank tests. T_a is air
 358 temperature, θ is soil moisture and GI is green index.

359

Variable	Partial-R ²	Probability (p)
T _a	0.190	<0.001
θ	0.037	0.002
GI	0.023	0.002

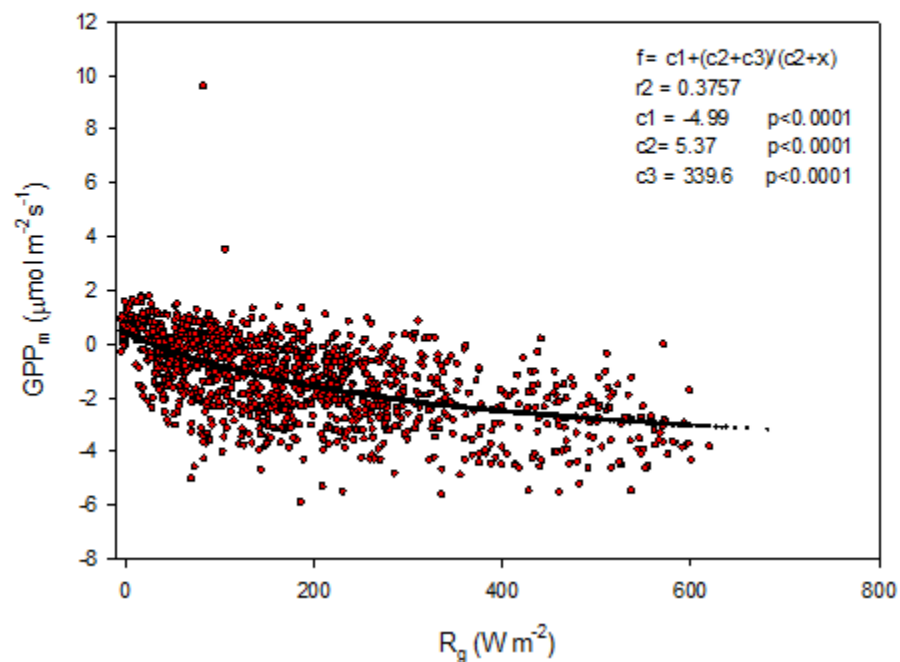
360
 361 Ideally all of these variables should be used in a model to estimate R_{eco} for gap filling purposes
 362 but we could only use air temperature since this was the only variable that we had access to with
 363 complete coverage for a full year. The Lloyd & Taylor model (Eq. 3 & Fig. 6)) was thus used to
 364 estimate ecosystem respiration for 2015 using half-hourly air temperature as input.



366 Figure 6. Measured ecosystem respiration (R_{eco}; green dots) plotted against air temperature. The
 367 red curve is the fitted equation and the blue curves are the corresponding boundaries when
 368 considering the standard deviation of the parameters.

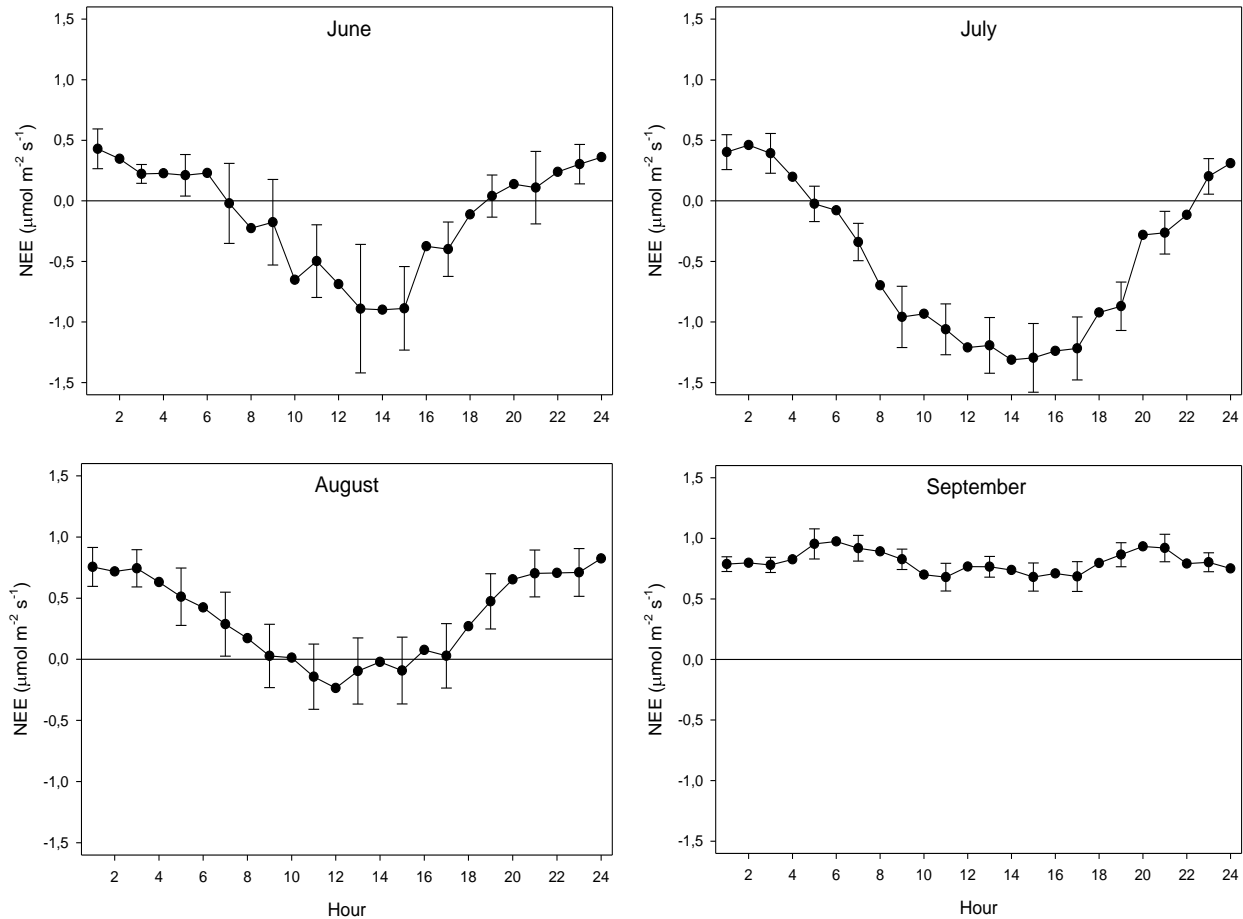
369

370 The modelled gross primary productivity (Eq. 6; GPP_m) had a small offset when global radiation
371 was zero (Fig. 7). This offset was adjusted for when the model was applied for gapfilling so that
372 GPP become zero during nighttime.



373
374
375 Figure 7. Gross primary productivity (GPP_m) plotted against global radiation (R_g) ; red symbols
376 are estimated values according to eq. (5) and the black symbols are the fitted model.

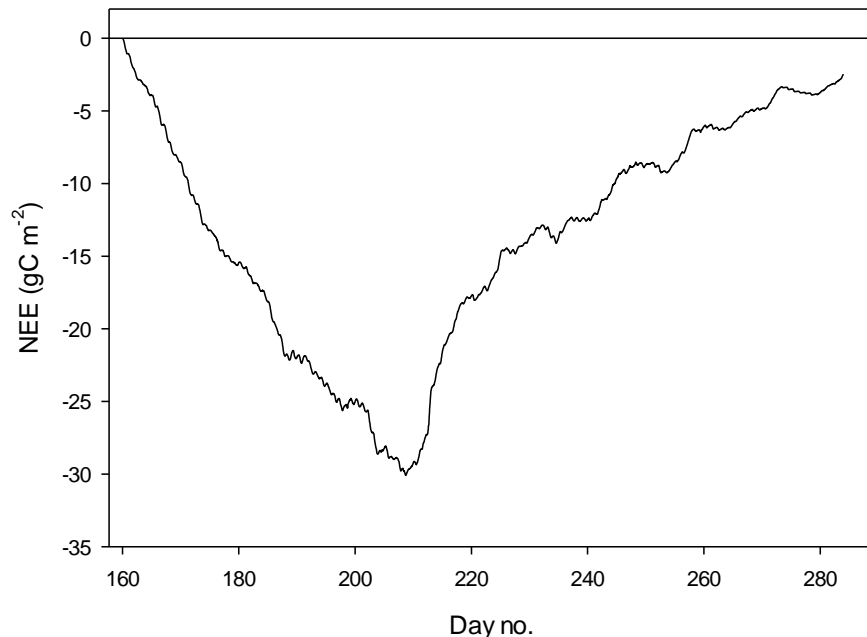
377
378
379
380
381



382
 383 Figure 8. The mean monthly diurnal course of net ecosystem exchange (NEE) during the period
 384 of eddy covariance measurements 25 June to 17 September. The error bars (every 2nd shown) are
 385 the 95% confidence interval. Notice that the main part of August was gap filled because of
 386 measurement problems.

387
 388
 389 The diurnal course of NEE during June - August exhibit the normal pattern with a successively
 390 increasing drawdown of CO₂ during first half of the day resulting in a maximum around noon. It
 391 should be noted that during June until 20 August the sun was over the horizon 24 hours, thus no
 392 dark period. The positive values at the beginning and end of the diurnal courses are a result of
 393 R_{ecco} being larger than GPP. As pointed out in Fig. 8, most of the data of August were gapfilled
 394 causing some additional uncertainty. However, the diurnal course seems reasonable although the
 395 peak during noon is much lower as compared to July. This can be explained by the much lower
 396 incoming radiation in August as compared to July; the mean global radiation in July was 192 W
 397 m⁻² and 98 W m⁻² in August. The mean air temperature was similar during July and August. In
 398 September the incoming radiation is very low and thus GPP is also very low which result in a
 399 NEE that is dominated by the R_{ecco}. The positive NEE values around mid-night during June –
 400 September are in good accordance with the values from the independent dark chamber
 401 measurements (Fig. 5).

402



403 Figure 9. The cumulated half-hourly net ecosystem exchange (NEE) during growing season.

404
405
406 The mean net CO₂ flux during the growing season was $-0.019 \pm 0.024 \mu\text{mol m}^{-2}\text{s}^{-1}$ with
407 uncertainty given as the 95% confidence limit. The cumulated NEE during growing season
408 ended up negative with -2.5 g C m^{-2} (Fig. 9). The mean net CO₂ flux during summer was -
409 $0.139 \pm 0.032 \mu\text{mol m}^{-2}\text{s}^{-1}$ (95% confidence limit) and the cumulated NEE was -11.8 g C m^{-2}
410 (Table 2).

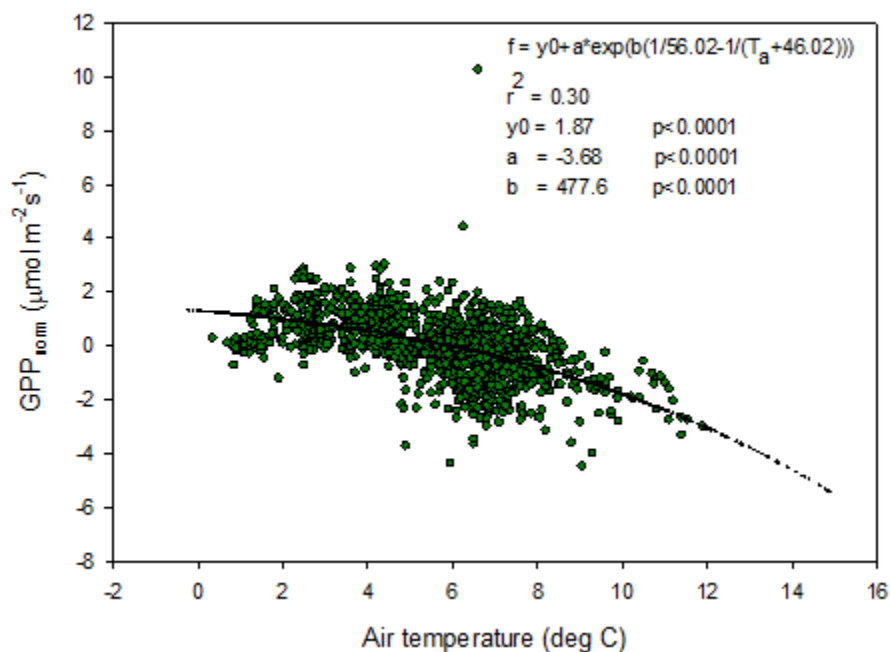
411
412 Table 2. Summary of seasonal C-fluxes from Kapp Linne. R_{eco} is ecosystem respiration, GPP is
413 gross primary productivity and NEE is net ecosystem exchange.

Period	Component	Value (gC m ⁻²)
Growing season	Reco	110.2
	GPP	-112.7
	NEE	-2.5
Summer	Reco	94.1
	GPP	-105.9
	NEE	-11.8

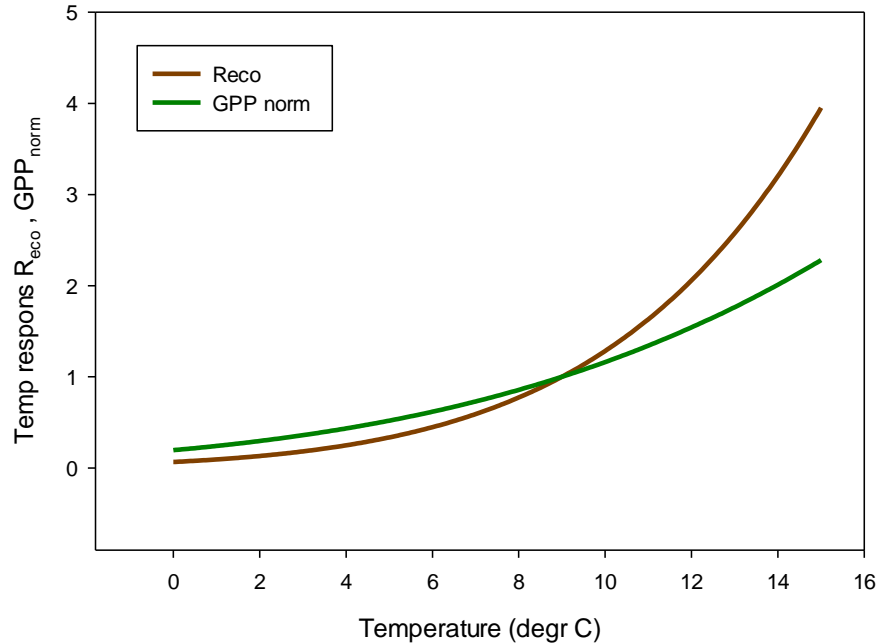
415 4.4 Temperature sensitivity of R_{eco} and GPP

416
417
418 The temperature sensitivity of the R_{eco} is already given by the fitted Lloyd & Taylor (1994)
419 equation. In the absence of long time series of measurements during multiple year were natural
420 climate variability could be used to assess temperature sensitivity of GPP we approached this
421 problem in the following way. We normalize GPP for its dependence on radiation by estimating
422 the difference between the ‘measured’ GPP and the model which only depends on radiation (see

423 Fig. 7). A stepwise linear regression with normalized GPP as dependent variable and air
 424 temperature, time of season and vapour pressure deficit as independent variables, showed that of
 425 the total explained variance, air temperature stood for 94% and time of season and vapour
 426 pressure deficit for 3% each. Thus, the resulting normalized GPP show effectively a dependence
 427 on air temperature (Fig. 10) with values becoming more negative, i.e. showing increasing GPP
 428 with increasing temperature. We fitted the same type of model to these data as for the R_{eco} to be
 429 able to compare sensitivities to temperature.



430 Figure 10. Normalized gross primary productivity (GPP) plotted against air temperature and with
 431 the fitted exponential model.
 432
 433



434
 435 Figure 11. Temperature sensitivity for ecosystem respiration (R_{eco}) (brown) and R_g -normalized
 436 (positive) gross primary productivity (GPP) (green).

437
 438 In Fig. 11 we reversed the sign of the GPP temperature response function to make it more easily
 439 comparable with the R_{eco} response model. The temperature sensitivity ($\mu\text{mol m}^{-2}\text{s}^{-1} \text{K}^{-1}$) can be
 440 estimated from the slope of these curves and the sensitivity is slightly higher for GPP than for
 441 R_{eco} in the interval 0 – 4.5 °C, thereafter the difference is small up to about 6 °C then it began to
 442 raise rapidly for R_{eco} . We tested what impact this could have by increasing the measured half-
 443 hourly air temperature by 1 °C and found that during the growing season the GPP increased by -
 444 31.9 g C m^{-2} and R_{eco} by 36.4 g C m^{-2} . Thus, a slightly larger increase of R_{eco} as compared to
 445 GPP resulting in that the small sink of -2.5 gC m^{-2} turns into a source of 4.5 gC m^{-2} .

446 447 4.5 CH_4 exchanges

448
 449 The CH_4 fluxes from the chamber measurements showed large variation over time (Fig. 12) and
 450 across sampling locations (Fig. 13). The mean CH_4 flux of all samples was 0.00051 ± 0.00024
 451 $\mu\text{mol m}^{-2}\text{s}^{-1}$. The uncertainty is given as the 95% confidence limit. Setting all fluxes that fell
 452 within the flux detection limits to zero changed the mean value with -0.2%. Assuming that the
 453 mean flux was representative for the whole of growing season 1, the total CH_4 summer emission
 454 was 0.039 to 0.164 $\text{g CH}_4 \text{m}^{-2}$.

455
 456 We also noticed a clear trend during the summer with highest fluxes in mid-June and then
 457 decreasing during the following two sampling occasions. The respective mean values with 95%
 458 confidence intervals for the three sampling periods were $0.00121 \pm 0.000512 \mu\text{mol m}^{-2}\text{s}^{-1}$ (June 14-
 459 15), $0.000332 \pm 0.000465 \mu\text{mol m}^{-2}\text{s}^{-1}$ (June 26- July 2) and $-0.00000781 \pm 0.0000936 \mu\text{mol m}^{-2}\text{s}^{-1}$
 460 (August 25-26).

461

462 For CH₄ exchanges we found *ALD*, θ and *GI* to contribute significantly to explain the variance of
 463 the flux (Table 3). The CH₄ flux responded negatively to increasing *ALD* and positively to θ and
 464 *GI*.

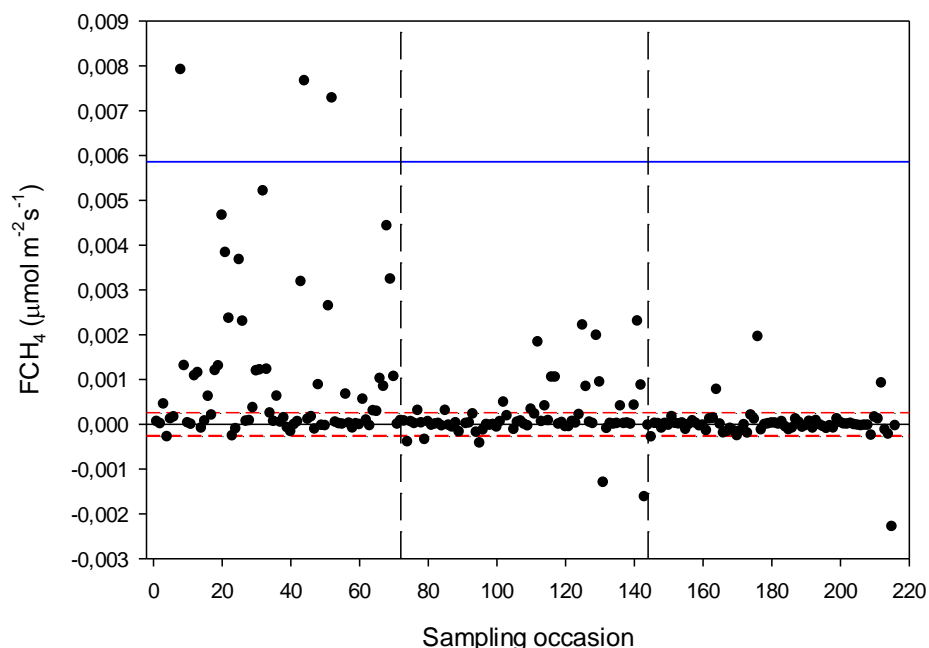
466 Table 3. Result of stepwise multiple linear regression with CH₄ flux as dependent variable.
 467 Normality test failed but significance in all variables was confirmed with Wilcoxon Signed rank
 468 tests. *ALD* is active layer depth, θ is soil moisture and *GI* is green index.

469

Variable	Delta-R ²	Probability (p)
<i>ALD</i>	0.175	<0.001
θ	0.025	0.01
<i>GI</i>	0.020	0.004

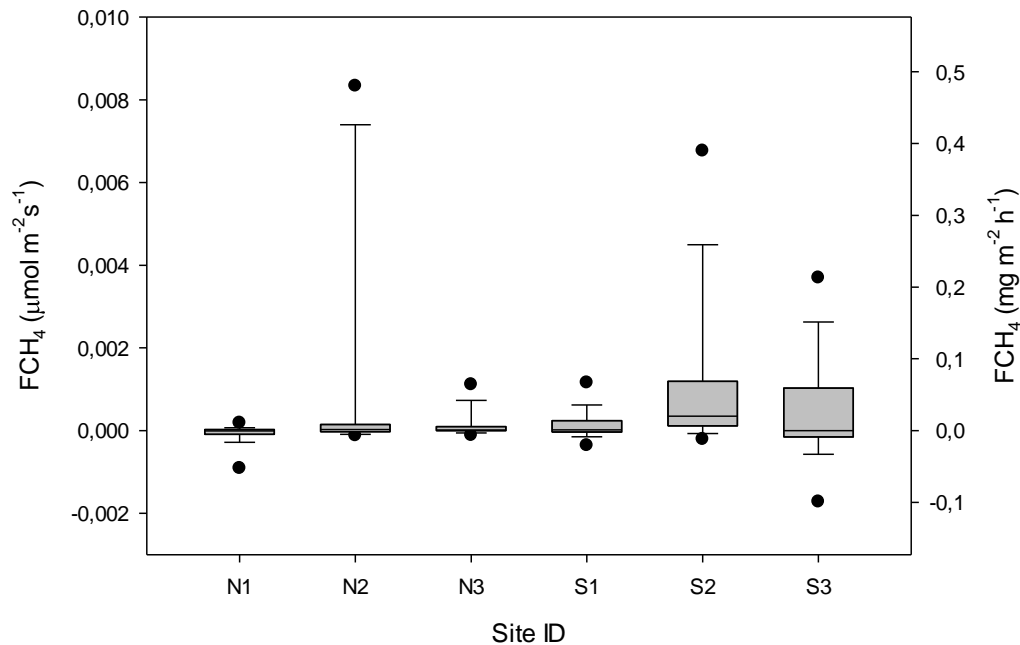
470

471



472

473 Figure 12. Measured CH₄ exchange (FCH₄) from the 24 sampling points using dark chamber and
 474 portable gas analyzer. The dashed red lines indicate CH₄ flux detection limit, (i.e. inside the
 475 limits of detection the exact numbers are highly uncertain) and the blue line represents 3xS.D.
 476 The dashed vertical lines – same as in Fig. 4.



477

478 Figure 13. Box plot of CH₄ fluxes (FCH₄) per sampling location named N1-N3, S1-S3. The
 479 statistics includes also the data that fall within the flux detection limits. The boundaries of the
 480 grey boxes represent the 25% and 75% percentiles, the line represent the median, whiskers above
 481 and below the boxes indicate the 10% and 90% percentiles. Outlying points are also shown.

482 5 Discussion

483 5.1 Seasonal CO₂ fluxes

484

485 We focus our discussion mainly on comparison with other tundra sites located in the North
 486 Atlantic area since these sites are influenced by the North Atlantic Current with its impact on
 487 weather patterns and climate. This limits the comparisons to sites in Greenland, Svalbard and
 488 Northern Scandinavia. However, we broaden the comparison a bit by adding two sites from
 489 Alaska.

490

491 Lund et al. (2012) found that the start of the uptake period was strongly correlated with start of
 492 the snowmelt for the fen in Zackenberg, NE Greenland. They defined the start of snowmelt as
 493 the day when snow depth was <0.1 m. This coincides very well with our definition of start of
 494 growing season (see Fig. 2). Our results for the growing season NEE showing a small net uptake
 495 of -2.5 g C m⁻² is at the low end in comparison with any other high arctic sites which all show a
 496 larger gain of carbon during the growing seasons.

497

498 Lund et al. (2012) analysed 10 years of EC flux measurements from a heathland in Zackenberg
 499 and they reported a NEE range of -39.7 to -4.3 g C m⁻² for the growing season. It was only two
 500 years out of ten that showed NEE values close to zero but still indicating a small net uptake in
 501 Zackenberg heath. Their measured growing season GPP was in the range of -95.4 to -54.1 g C m⁻²
 502 and the R_{eco} was in the range of 37.7 to 63.8 g C m⁻². Our corresponding values were -112.7 g

503 C m⁻² for GPP and 110.2 g C m⁻² for R_{eco}. López-Blanco et al. (2017) presented data over a
504 period of eight years of EC flux measurements from Kobbefjord, SW Greenland over an area of
505 mixed fen and heath vegetation. Their growing season ranges were; for NEE -74.2 to -45.9 g C
506 m⁻², for GPP -316.2 to -181.8 g C m⁻² and for R_{eco} it was 144.2 to 279.2 g C m⁻² excluding 2011
507 which was anomalous because of a pest outbreak and 2014 which did not have a full growing
508 season.

509
510 Our estimate of a small summer NEE of -11.8 g C m⁻² (Table 2) is also different in comparison
511 with other tundra sites which show larger uptake during the summer; for a fen type of vegetation
512 in NE Greenland Soegaard and Nordstroem (1999) reported -96.3 g C m⁻² while Rennermalm et
513 al. (2005) reported -50 g C m⁻² for the same site but for a different year. Groendahl et al. (2007)
514 reported a range of -1.4 to -18.9 g C m⁻² for heath vegetation also on NE Greenland.

515
516 It is difficult to compare growing season values firstly because they are rarely defined the same
517 way. Only small differences in definition of start and end of growing season can have a large
518 impact on the NEE values since NEE is the sum of two large components of almost equal size
519 and of different sign. Secondly, it is also difficult to compare GPP and R_{eco} for any season since
520 the methods to split NEE into components differ from case to case. The most reliable comparison
521 is probably for summer season (June – August) since most studies represents this period best in
522 terms of measurement coverage and quality. And thirdly, there are differences in vegetation type
523 that can have a big impact on gas exchanges. Our moist moss tundra is dominated by moss
524 species and mosses are not as efficient primary producers as vascular plants and this make the
525 net uptake of carbon dioxide small as compared to heath or wet fen systems.

526
527 The climate warming is predicted to be most evident at high latitudes such as the Arctic region.
528 Svalbard has experienced significant warming during the last decades (1971-2017) with 3- 5
529 degrees with the largest increase in the winter and smallest in the summer (Hanssen-Bauer et al.,
530 2019). Our air temperature observations in 2015 are in line with these results (Fig.1). An
531 interesting question is if such changes in temperature has also affected the net carbon balance of
532 the ecosystem? Our analysis of temperature sensitivity of R_{eco} and GPP shows that this could be
533 the case for this site since R_{eco} is increasing more than GPP for temperatures above about 6 °C
534 which occurs quite frequent during the summer (see Fig. 2). Our analyses of the impact of a
535 temperature increase of 1 °C showed that our small sink of -2.5 g C m⁻² during growing season
536 would be turned into a similarly small source of 4.5 g C m⁻² for a 1 degree increase in air
537 temperature. These results are in line of those of Welker et al. (2004) who performed a warming
538 experiment in high Arctic tundra ecosystems. They showed that the net ecosystem exchange in
539 the wet tundra ecosystem decreased by 20% during growing season under a 2 degree warming
540 treatment. This was in contrast to the dry and mesic ecosystems which increased their net carbon
541 uptake by 12-30%.

542
543

544 5.2 CH₄ fluxes

545
546 Our estimated growing season CH₄ flux of 0.08 g C m⁻² is very low compared to most other
547 methane emitting tundra sites; the Zackenberg fen site emitted CH₄ in the range 1.4 to 4.9 g C m⁻²
548 (Mastepanov et al. (2013), Jackowicz-Korczynski et al. (2010) and Jammet et al. (2015)

549 reported 20.1 to 25.1 g CH₄ m⁻² for the Stordalen mire in Northern Sweden. For three different
550 sites in northern Alaska, Bao et al. (2021) reported annual emissions between 1.8 and 8.5 g CH₄
551 m⁻² which corresponds to 0.94 and 4.5 g CH₄ m⁻² for the growing season based on their estimate
552 that growing season emissions are 52.6% of the annual emissions. Sachs et al. (2008) measured
553 CH₄ exchanges with EC method in a northern Siberian polygon tundra and found generally low
554 fluxes of about 18.5 mg CH₄ m⁻² day⁻¹ with little variation over the growing season. This rate
555 adds up to 2.3 g CH₄ m⁻² for their four months long growing season.

556
557 It should be pointed out that we did not perform measurements during the shoulder seasons
558 meaning that we probably underestimate the seasonal total. Importance of shoulder seasons was
559 first pointed out by Mastepanov et al. (2008) which discovered a large burst of CH₄ at and after
560 the onset of soil freezing. One interesting observation is that the main part of our CH₄ flux
561 occurred during the sampling period 14-15 June 2016 which is about 30 days after snow melt.
562 This is the time of the season when CH₄ emissions normally are peaking (Mastepanov et al.
563 2013). After that, the rates dropped to practically zero in late August (see Fig. 12).

564
565
566 The comparison between the different sites are hampered by the fact that they in most cases
567 belong to different bioclimatic subzones with differences in climate and vegetation (Walker et
568 al., 2005). The only site besides Kapp Linne that belong to subzone B is the one in Ny Ålesund.
569 The other high Arctic sites Adventdalen and Zackenberg both belong to subzone C, the
570 intermediate high/low Arctic sites Kobbefjord and Disco Island belongs to subzone D
571 respectively C/D. The low Arctic site Atqasuk belong to subzone D and the Imnavait Creek
572 belong to subzone E. The sub-Arctic Abisko is not classified by Walker et al. (2005) but based
573 mean July air temperature it should belong to subzone E. These differences in climate and
574 vegetation should be kept in mind when comparing results from different sites.

575 576 5.3 Environmental controls of fluxes

577
578 A key issue in high Arctic is how ecosystems with soil that contain large amounts of frozen
579 carbon will respond to warming. A recent report about the future climate of Svalbard (Hanssen-
580 Bauer et al. 2019) show that appalling changes are at risk to occur. By 2071-2100 compared to
581 1971-2000 the mean annual temperature is estimated to increase by 7 °C to 10 °C for the medium
582 and high emission scenarios, respectively. Precipitation is also estimated to increase by 45%
583 respectively 65% for these scenarios. Such large changes will of course also have a lot of other
584 impacts as well for instance shorter snow season, more erosion and sediment transport, changes
585 in vegetation composition and growth etc etc. Assessment of such large changes are very
586 difficult and is far beyond the scope of this paper. We have however shown that for a smaller
587 temperature increase of 1 degree, the impact on the net carbon balance during the growing
588 season will be minute; the increase in ecosystem respiration is compensated for by a
589 corresponding, or actually slightly larger increase of gross primary productivity. Similar
590 compensation effect was obtained for a heath site in Zackenberg by Lund et al. (2012). They
591 used multi-year measurements to assess the effect of changes in temperature on the growing
592 season fluxes

593

594 We found that air temperature was the main control of ecosystem respiration followed by soil
595 moisture and greenness index (Table 1). We had expected that soil temperature should contribute
596 significantly to explain the variations in R_{eco} but it did not. Cannone et al. (2019) showed that
597 ground surface temperature at 2 cm depth contributed significantly to explain R_{eco} in nearby
598 Adventdalen during early, peak and late parts of the growing season. In their study soil moisture
599 was also significant during peak and late seasons. One possible explanation to this difference in
600 responses could be that our soil temperature was measured at 5 cm depth and that air temperature
601 was more representative for the microbial processes taking place in or near the soil surface.
602 Interestingly, GI contributed significantly to explain variations in R_{eco} . The GI was clearly
603 correlated with the abundance of *Salix polaris* (see Supplement) and thus we interpret the
604 positive correlation between GI and R_{eco} to be an effect of increasing contribution by autotrophic
605 respiration to the total respiration.

606 We found no significant correlation between CH_4 emission and temperature. The best
607 explanation was by active layer depth followed by soil moisture and GI (Table 3). But it should
608 be pointed out that ALD and θ are not independent from each other and that ALD can be
609 regarded as a proxy for any seasonal variability, like plant phenology. Soil moisture decreases
610 with increasing active layer depth. The correlation between GI and CH_4 emission is probably
611 also connected with abundance of the vascular plant *Salix polaris*. Vascular plants are since long
612 mentioned as a pathway for CH_4 from the soil interior to the atmosphere in wet tundra
613 ecosystems (e.g. Schimel, 1995) but it could also be an effect of mediation of soil by the root
614 exudation of organic acids as mentioned by Ström et al. (2012). However, we have not found any
615 studies supporting the latter hypothesis concerning *Salix polaris*.

616 **6 Conclusions**

617 Our analyses of EC and chamber flux measurements have shown that the moss tundra on Kapp
618 Linne is a small sink of CO_2 and a small source of CH_4 during the growing season. Realizing that
619 the winter season also emit CO_2 , we tentatively conclude that this moist moss tundra is a source
620 on an annual basis. Concerning the magnitude of the CO_2 exchanges during summer we find it to
621 be anomalous compared to fens and heath ecosystems located in the North Atlantic region
622 which all are sinks during the summer. The CH_4 exchange is much lower than for other tundra
623 ecosystems in the region.

624
625 The temperature sensitivity for CO_2 exchange was slightly higher for GPP than for R_{eco} in the
626 low temperature range of 0-4.5 °C, almost similar up to 6 °C and thereafter it was considerably
627 higher for R_{eco} . The consequence of this, for a small increase in air temperature of 1 degree (all
628 other variables assumed unchanged) was that the respiration increased more than photosynthesis
629 turning the small sink into a small source. But a warmer winter period would probably also result
630 in an additionally increased loss of carbon. We cannot rule out that the reason why the moss
631 tundra is close to balance today is an effect of the warming that has already taken place in
632 Svalbard.

633 The analysis of which environmental factors that controlled the small-scale fluxes showed that
634 air temperature dominated for R_{eco} and active layer depth for CH_4 but we also found that
635 greenness index significantly explained part of the variation in these fluxes. For R_{eco} we
636 attributed this to an increased share of autotrophic respiration to the total and for CH_4 we

637 hypothesized that the abundance of the dwarf shrub *Salix polaris* effected the exchange either
638 through internal plant pathway for methane or through increased provision of C substrate to the
639 anaerobic microbial community stimulating the production of methane. This finding is an
640 indication that modeling of CO₂ as well as of CH₄ fluxes can be improved by also considering
641 differences and changes in greenness of the vegetation.

642 **7 Supplement**

643 The supplement contains some additional photographs of equipment, site and color photographs
644 of vegetation within the frames used for chamber measurements.

645 **8 Data availability**

646 Data can be obtained from <https://zenodo.org> ([10.5281/zenodo.5704508](https://zenodo.org/record/10.5281/zenodo.5704508)).

647 **9 Author contribution**

648 AL designed the study and wrote the manuscript. NP and AL performed the EC measurements
649 and analysed the EC data. ISJ did the vegetation characterization. AL, CS, LK and MBN
650 performed the chamber measurements. All authors have read and commented the manuscript.

651 **10 Competing interests**

652 We declare no competing interests.

653 **11 Acknowledgments**

654 This work did not receive any other funding except salaries for the authors from their respective
655 organizations. Observations of air temperature, relative humidity, precipitation, ground ice
656 conditions and snow depth were obtained from Norwegian Centre for Climate Services (NCCS)
657 and provided under licence CC BY 4.0. Global radiation data from Adventdalen was obtained
658 from the University Centre in Svalbard (UNIS). Thanks to associated professor Jonas Åkerman,
659 Lund University for support with information about the site.

660

661 **12 References**

662 Arias, P. A., Bellouin, E., Coppola, R.G. et al.: Technical Summary, in: Climate Change 2021:
663 The Physical Science Basis. Contribution of Working Group I to the Sixth Assessment
664 Report of the Intergovernmental Panel on Climate Change, edited by: Masson-Delmotte,
665 V., P. Zhai, A. Pirani, S. L. Connors, C. Péan, S. Berger, N. Caud, Y. Chen, L. Goldfarb,
666 M. I. Gomis, M. Huang, K. Leitzell, E. Lonnoy, J.B.R. Matthews, T. K. Maycock, T.
667 Waterfield, O. Yelekçi, R. Yu and B. Zhou, Cambridge University Press, In Press, 2021.

668 Bao, T., Xu, X., Jia, G., Billesbach, D.P. and Sullivan, R.C.: Much stronger tundra methane
669 emissions during autumn freeze than spring thaw, *Global Change Biology*, 27, 376–387,
670 [https://doi.org/ 10.1111/gcb.15421](https://doi.org/10.1111/gcb.15421), 2021

671 Bosiö, J., Stiegler, C., Johansson, M., Mbufong, H. N. and Christensen, T. R.: Increased
672 photosynthesis compensates for shorter growing season in subarctic tundra—8 years of

673 snow accumulation manipulations, *Climatic Change*, 127, 321–334,
674 <http://doi.org/10.1007/s10584-014-1247-4>, 2014.

675 Burba, G. G., McDermitt, D., Grelle, A., Anderson, D.J. and Xu, L.: Addressing the influence of
676 instrument surface heat exchange on the measurements of CO₂ flux from open-path gas
677 analyzers, *Global Change Biology*, 14, 1854–1876, [https://doi.org/10.1111/j.1365-](https://doi.org/10.1111/j.1365-2486.2008.01606.x)
678 [2486.2008.01606.x](https://doi.org/10.1111/j.1365-2486.2008.01606.x), 2008.

679 Callaghan, T.V., Björn, L O., Chapin III, F.S., Chernov, Y., Christensen, T.R., Huntley, B., Ims,
680 R., Johansson, M., Jolly Riedlinger, D., Jonasson, S., Matveyeva, N., Oechel, W.,
681 Panikov, N. and Shaver, G.: Arctic tundra and polar desert ecosystems, in: *Arctic Climate*
682 *Impact Assessment*, edited by: ACIA, Cambridge University Press, 243-352, 2005.

683 Cannonea, N., Pontib, S., Christiansen, H.H., Christensen, T.R., Pirk, N. and Guglielmin, M.:
684 Effects of active layer seasonal dynamics and plant phenology on CO₂ land atmosphere
685 fluxes at polygonal tundra in the High Arctic, Svalbard, *Catena*, 174, 142-153,
686 <https://doi.org/10.1016/j.catena.2018.11.013>, 2019.

687 Christensen, T.R., Johansson, T., Akerman, H.J. and Mastepanov, M.: Thawing sub-arctic
688 permafrost: Effects on vegetation and methane emissions, *Geophysical Research Letters*,
689 31, L04501, <https://doi.org/10.1029/2003GL018680>, 2004.

690 Christensen, T.R., Jackowicz-Korzynski, M., Aurela, M., Crill, P., Heliasz, M., Mastepanov, M.
691 and Friborg, T.: Monitoring the Multi-Year Carbon Balance of a Subarctic Palsa Mire
692 with Micrometeorological Techniques, *Ambio*, 41, 207–217,
693 <https://doi.org/10.1007/s13280-012-0302-5>, 2012.

694 Dobler, A., Lutz, J., Landgren, O. and Haugen, J. E.: Circulation Specific Precipitation Patterns
695 over Svalbard and Projected Future Changes, *Atmosphere*, 11, 1378;
696 [doi:10.3390/atmos11121378](https://doi.org/10.3390/atmos11121378), 2021.

697

698 Euskirchen, E. S., Bret-Harte, M. S., Scott, G. J., Edgar, C., and Shaver, G. R.: Seasonal patterns
699 of carbon dioxide and water fluxes in three representative tundra ecosystems in northern
700 Alaska, *Ecosphere*, 3, 1–19, <https://doi.org/10.1890/ES11-00202.1>, 2012.

701

702 Euskirchen, E.S., Bret-Harte, M.S., Shaver, G.R., Edgar, C.W., and Romanovsky, V.E.: Long-
703 Term Release of Carbon Dioxide from Arctic Tundra Ecosystems in Alaska, *Ecosystems*,
704 20, 960–974, <http://doi.org/10.1007/s10021-016-0085-9>, 2017.

705 Friedlingstein, P., Cox, P., Betts, R., Bopp, L., von Bloh, W., Brovkin, V., Cadule, P., Doney, S.,
706 Eby, M., Fung, I., Bala, G., John, J., Jones, C., Joos, F., Kato, T., Kawamiya, M., Knorr,
707 W., Lindsay, K., Matthews, H. D., Raddatz, T., Rayner, P., Reick, C., Roeckner, E.,
708 Schnitzler, K. G., Schnur, R., Strassmann, K., Weaver, A. J., Yoshikawa, C., and Zeng,

- 709 N.: Climate-carbon cycle feedback analysis: Results from the C4MIP model
710 intercomparison, *J. Climate*, 19, 3337–3353, <https://doi.org/10.1175/JCLI3800.1>, 2006.
- 711 Friedlingstein, P., O’Sullivan, M., Jones, M.W. et al.: Global carbon budget 2010, *Earth Syst.*
712 *Sci. Data*, 12, 3269–3340, <https://doi.org/10.5194/essd-12-3269-2020>, 2019.
- 713 Groendahl, L., Friborg, T., and Soegaard, H.: Temperature and snow-melt controls on
714 interannual variability in carbon exchange in the high Arctic, *Theor. Appl. Climatol.*, 88,
715 111–125, <http://doi.org/10.1007/s00704-005-0228-y>, 2007.
- 716 Hanssen-Bauer, I., Førland, E.J., Hisdal, H., Mayer, S., Sandø, A.B. and Sorteberg, A.: Climate in
717 Svalbard 2100 – a knowledge base for climate adaptation, Norwegian Environment
718 Agency, Report no. 1/2019., 2019.
- 719 Hugelius, G., Strauss, J., Zubrzycki, S., Haren, J.W., Schuur, E.A.G., Ping, C.-L., Schirrmeister,
720 L., Grosse, G., Michaelson, G.J., Koven, C.D., O’Donnell, J.A., Elberling, B., Mishra,
721 U., Camill, P., Yu, Z., Palmtag, J. and Kuhry, P.: Estimated stocks of circumpolar
722 permafrost carbon with quantified uncertainty ranges and identified data gaps,
723 *Biogeosciences*, 11, 6573–6593, <http://doi.org/10.5194/bg-11-6573-2014>, 2014.
- 724 Jackowicz-Korczynski, M., Christensen, T. R., Backstrand, K., Crill, P., Friborg, T.,
725 Mastepanov, M. and Strom, L.: Annual cycle of methane emission from a subarctic
726 peatland, *J. Geophys. Res.-Biogeo.*, 115, G02009, <http://doi.org/10.1029/2008JG000913>,
727 2010.
- 728 Jammet, M., Crill, P., Dengel, S. and Friborg, T.: Large methane emissions from a subarctic
729 lake during spring thaw: Mechanisms and landscape significance. *J. Geophys. Res.-*
730 *Biogeo.*, 120, 2289-2305, <http://doi.org/10.1002/2015JG003137>, 2015.
- 731 Kljun, N., Calanca, P., Rotach, M.W., and Schmid, H.P.: A simple two-dimensional
732 parameterisation for Flux Footprint Prediction (FFP), *Geosci. Model Dev.*, 8, 3695-3713,
733 <http://doi.org/10.5194/gmd-8-3695-2015>, 2015.
- 734 Lasslop, G., Reichstein, M., Papale, D., Richardson, A., Arneth, A., Barr, A., Stoy, P. and
735 Wohlfahrt, G.: Separation of net ecosystem exchange into assimilation and respiration
736 using a light response curve approach: critical issues and global evaluation. *Global*
737 *Change Biology*, 16, 187-208, <https://doi.org/10.1111/j.1365-2486.2009.02041.x>, 2010.
- 738 Li-Cor: EddyPro® Software (Version 6.0), Li-Cor Inc., Lincoln, USA, 2016.
- 739 Lloyd, J., and Taylor, J.A.: On the temperature dependence of soil respiration, *Functional*
740 *Ecology*, 8(3), 315-323, 1994.
- 741 Lopez-Blanco, E., Lund, M., Williams, M., Tamstorf, M.P., Westergaard-Nielsen, A., Exbrayat,
742 J.-F., Hansen, B.U., and Christensen, T.R.: Exchange of CO₂ in Arctic tundra: impacts of

- 743 meteorological variations and biological disturbance, *Biogeosciences*, 14, 4467–4483,
744 <https://doi.org/10.5194/bg-14-4467-2017>, 2017.
- 745 Lund, M., Falk, J. M., Friborg, T., Mbufong, H. N., Sigsgaard, C., Soegaard, H., and Tamstorf,
746 M. P.: Trends in CO₂ exchange in a high Arctic tundra heath, 2000–2010, *J. Geophys.*
747 *Res.- Biogeo.*, <https://doi.org/10.1029/2011JG001901>, 2012.
- 748 Lüers, J., Westermann, S., Piel, K., and Boike, J.: Annual CO₂ budget and seasonal CO₂
749 exchange signals at a high Arctic permafrost site on Spitsbergen, Svalbard archipelago,
750 *Biogeosciences*, 11, 6307–6322, <http://doi.org/10.5194/bg-11-6307>, 2014.
- 751 Mastepanov, M., Sigsgaard, C., Dlugokencky, E. J., Houweling, S., Strom L., Tamstorf, M. P.,
752 and Christensen, T. R.: Large tundra methane burst during onset of freezing, *Nature*, 456,
753 628–631, <http://doi.org/10.1038/nature07464>, 2008.
- 754 Mastepanov, M., Sigsgaard, C., Tagesson, T., Ström, L., Tamstorf, M. P., Lund, M., and
755 Christensen, T. R.: Revisiting factors controlling methane emissions from high-Arctic
756 tundra, *Biogeosciences*, 10, 5139–5158, <https://doi.org/10.5194/bg-10-5139-2013>, 2013.
- 757 McGuire, A. D., Christensen, T. R., Hayes, D., Heroult, A., Euskirchen, E., Kimball, J. S.,
758 Koven, C., Lafleur, P., Miller, P. A., Oechel, W., Peylin, P., Williams, M., and Yi, Y.: An
759 assessment of the carbon balance of Arctic tundra: comparisons among observations,
760 process models, and atmospheric inversions, *Biogeosciences*, 9, 3185–3204,
761 <https://doi.org/10.5194/bg-9-3185-2012>, 2012.
- 762 Myers-Smith, I. H., Kerby, J. T., Phoenix, G. K., Bjerke, J. W., Epstein, H. E., Assman, J. J.,
763 John, C., Adreu-Hayles, L., Angers-Blondin, S., Beck, P. S. A., Berner, L. T., Bhatt, U.
764 S., Bjorkman, A. D., Blok, D., Bryn, A., Christiansen, C. T., Cornelissen, J. H. C.,
765 Cunliffe, A. M., Elmendorf, S. C., Forbes, B. C., Goetz, S. J., Hollister, R. D., de Jong,
766 R., Loranty, M. M., Marcias-Fauria, K., Maseyk, K., Normand, S., Olofsson, J., Parker,
767 T. C., Parmentier, F.-J. W., Post, E., Schaepman-Strub, G., Stordal, F., Sullivan, P. F.,
768 Thomas, H. J. D., Tømmervik, H., Treharne, R., Tweedie, C. E., Walker, D. A.,
769 Wilmking, M. and Wipf, S.: Complexity revealed in the greening of the Arctic, *Nat.*
770 *Clim. Chang.*, 10, 106–117, <https://doi.org/10.1038/s41558-019-0688>, 2020.
- 771 Oechel, W. C., C. A. Laskowski, G. Burba, B. Gioli, and Kalhori, A.A.M.: Annual patterns and
772 budget of CO₂ flux in an Arctic tussock tundra ecosystem, *J. Geophys. Res. Biogeo.*,
773 119, 323–339, <http://doi.org/10.1002/2013JG002431>, 2014.
- 774 Pastorello, G., Trotta, C., Canfora, E. et al.: The FLUXNET2015 dataset and the ONEFlux
775 processing pipeline for eddy covariance data, *Sci Data*, 7, 225,
776 <https://doi.org/10.1038/s41597-020-0534-3>, 2020.
- 777 Pirk, N., Sievers, J., Mertes, J., Parmentier, F.-J. W., Mastepanov, M., and Christensen, T. R.:
778 Spatial variability of CO₂ uptake in polygonal tundra: assessing low-frequency

- 779 disturbances in eddy covariance flux estimates, *Biogeosciences*, 14, 3157–3169,
780 <https://doi.org/10.5194/bg-14-3157-2017>, 2017.
- 781 Post, E., Forchhammer, M. C., Bret-Harte, M. S., Callaghan, T. V., Christensen, T. R., Elberling,
782 B., Fox, A. D., Gilg, O., Hik, D. S., Høye, T. T., Ims, R. A., Jeppesen, E., Klein, D. R.,
783 Madsen, J., McGuire, A. D., Rysgaard, S., Schindler, D. E., Stirling, I., Tamstorf, M. P.,
784 Tyler, N. J. C., van der Wal, R., Welker, J., Wookey, P. A., Schmidt, M. and Astrup, P.:
785 Ecological dynamics across the arctic associated with recent climate change, *Science*,
786 325, 1355–1358, <http://doi.org/10.1126/science.1173111>, 2009.
- 787 Ravolainen, V., Soininen, E. M., Jónsdóttir, I. S., Eischeid, I., Forchhammer, M., van der Wal,
788 R. and Pedersen, A. Ø.: High Arctic ecosystem states: Conceptual models of vegetation
789 change to guide long-term monitoring and research, *Ambio*, 49, 666–677,
790 <https://doi.org/10.1007/s13280-019-01310-x>, 2020.
- 791 Rennermalm, A.K., Soegaard, H., and Nordstroem, C.: Interannual Variability in Carbon
792 Dioxide Exchange from a High Arctic Fen Estimated by Measurements and Modeling,
793 *Arctic, Antarctic, and Alpine Research*, 37(4), 545-556, [https://doi.org/10.1657/1523-
794 0430\(2005\)037\[0545:IVICDE\]2.0.CO;2](https://doi.org/10.1657/1523-0430(2005)037[0545:IVICDE]2.0.CO;2), 2005.
- 795 Richardson, A. D., Braswell, B. H., Hollinger, D. Y., Jenkins, J. P. and Ollinger, S. V.: Near-
796 surface remote sensing of spatial and temporal variation in canopy phenology, *Ecological*
797 *Applications*, 19, 1417–1428, <http://doi.org/10.1890/08-2022.1>, 2009.
- 798 Sachs, T., Wille, C., Boike, J., and Kutzbach, L.: Environmental controls on ecosystem-scale
799 CH₄ emission from polygonal tundra in the Lena river delta, Siberia, *J. Geophys. Res.-*
800 *Biogeosci.*, 113, G00A03, <http://doi.org/10.1029/2007JG000505>, 2008.
- 801 Saunio, M., Stavert, A.R., Poulter, B et al.: The global methane budget 2000-2017, *Earth Syst.*
802 *Sci. Data*, 12, 1561–1623, <https://doi.org/10.5194/essd-12-1561>, 2020.
- 803 Schimel, J.P.: Plant Transport and Methane Production as Controls on Methane Flux from Arctic
804 Wet Meadow Tundra, *Biogeochemistry*, 28 (3), 183-200,
805 <https://doi.org/10.1007/BF02186458>, 1995.
- 806 Schuur, E. A. G., McGuire, A. D., Schadel, C., Grosse, G., Harden, J. W., Hayes, D. J.,
807 Hugelius, G., Koven, C. D., Kuhry, P., Lawrence, D. M., Natali, S. M., Olefeldt, D.,
808 Romanovsky, V. E., Schaefer, K., Turetsky, M. R., Treat, C. C., and Vonk, J. E.: Climate
809 change and the permafrost carbon feedback, *Nature*, 520, 171–179,
810 <https://doi.org/10.1038/nature14338>, 2015.
- 811 Soegaard, H. & Nordstroem, C.: Carbon dioxide exchange in a high-arctic fen estimated by eddy
812 covariance measurements and modeling, *Glob. Change Biol.*, 5, 547–562,
813 <https://doi.org/10.1111/j.1365-2486.1999.00250.x>, 1999.

814 Strom, L., Tagesson, T., Mastepanov, M., and Christensen, T. R.: Presence of *Eriophorum*
815 *scheuchzeri* enhances substrate availability and methane emission in an Arctic wetland,
816 *Soil Biol. Biochem.*, 45, 61–70, <http://doi.org/10.1016/j.soilbio.2011.09.005>, 2012.

817
818 Walker, D. A., Raynolds, M. K., Daniëls, F. J. A., Einarsson, E., Elvebakk, A., Gould, W. A.,
819 Katenin, A. E., Kholod, S. S., Markon, C. J., Melnikov, E. S., Moskalenko, N. G., Talbot,
820 S. S., Yurtsev, B. A. and the other members of the CAVM Team: The Circumpolar
821 Arctic vegetation map, *Journal of Vegetation Science*, 16, 267-282,
822 <https://doi.org/10.1111/j.1654-1103.2005.tb02365.x>, 2005.

823 Welker, J.M., Fahnestock, J.T., Henry, G.H.R., O’Dea, K.W. and Chimner, R.A.: CO₂ exchange
824 in three Canadian High Arctic ecosystems: response to long-term experimental warming.
825 *Global Change Biology*, 10, 1981-1995. Doi: 1011/j.1365-2486.2004.00857.x, 2004.

826
827 Vanderpuye, A. W., Elvebakk, A. and Nilsen, L.: Plant communities along environmental
828 gradients of high-arctic mires in Sassendalen, Svalbard, *J. Veg. Sci.*, 13, 875–884,
829 <http://doi.org/10.1111/j.1654-1103.2002.tb02117.x>, 2002.

830
831 Vickers, H., Karlsen, S. R. and Malnes, E.: A 20-Year MODIS-Based Snow Cover Dataset for
832 Svalbard and Its Link to Phenological Timing and Sea Ice Variability, *Remote Sens.*, 12,
833 1123; doi:10.3390/rs12071123, 2020.

834
835
836 Wutzler, T., Lucas-Moffat, A., Migliavacca, M., Knauer, J., Sickel, K., Šigut, L., Menzer, O. and
837 Reichstein, M.: Basic and extensible post-processing of eddy covariance flux data with
838 REddyProc, *Biogeosciences*, 15(16), 5015-5030, Doi:10.5194/bg-15-5015-2018, 2018.

839 Zhang, W., Jansson, P-E., Sigsgaard, C., McConnella, A., Jammet, M.M., Westergaard-Nielsen,
840 A., Lund, M., Friberg, T., Michelsen, A., and Elberling, B.: Model-data fusion to assess
841 year-round CO₂ fluxes for an arctic heath ecosystem in West Greenland (69°N),
842 *Agricultural and Forest Meteorology*, 272-273, 176-186,
843 <https://doi.org/10.1016/j.agrformet.2019.02.021>, 2019.